International Journal of
MATERIALS RESEARCH

Zeitschrift für METALLKUNDE

Original Contributions

Serkan Abalı[a], Songül Kılınç[b]
[a]Department of Materials Science and Engineering, Çanakkale Onsekiz Mart University, Çanakkale, Turkey
[b]Department of Bioengineering and Materials Engineering, Çanakkale Onsekiz Mart University, Çanakkale, Turkey

Effects of sintering temperature on the microstructural properties of Al_2O_3–Y_2O_3 powder mixtures

Abstract: In this study, $YAlO_3$ (YAP) was produced at low temperatures by a powder sintering process. Al_2O_3–Y_2O_3 powder mixtures were subjected to heat treatment at different temperatures. The relationship between the sintering temperature and the emergence of new phases was investigated via X-ray diffraction, and supported by energy dispersive X-ray spectroscopy. The crystallization of the monoclinic yttrium aluminum oxide ($Y_4Al_2O_9$) occurred at 1 000 °C, whereas the yttrium aluminum perovskite ($YAlO_3$) crystallization occurred at 1 100 °C. Energy dispersive X-ray spectroscopy analysis showed yttrium content in the sample containing Al_2O_3–$YAlO_3$ powder sintered at 1 100 °C, associated with the $YAlO_3$ phase formed at this temperature. Brunauer–Emmett–Teller surface analysis showed a significant decrease in the pore volume of the sample sintered at 1 100 °C.

Keywords: Sintering; Al_2O_3; Y_2O_3; Powder

1 Introduction

Today, the main issue in ceramic production is the development of powder properties for a useful final product. The physical properties of materials can be improved by the powder sintering process [1]. Olmos et al. [2] studied the physical properties obtained by sintering a powder mixture without forming. It is known that powder properties are important for densification kinetics [2, 3]. Zhang and Saito characterized powder mixtures of Al_2O_3, $Al(OH)_3$ and Y_2O_3, all calcined at high temperatures, identifying $Y_3Al_5O_{12}$ (yttrium aluminum garnet) powders as the final product [4]. Studies exist in which powders are pre-sintered or calcined at high temperatures prior to forming. Lin et al. pre-sintered powders to increase the activity of hexagonal boron nitride (h-BN) [5]. Similarly, Yu et al. used a pre-sintering process to produce low-cost, high-performance composites [6]. The properties of the calcined powders prior to forming can provide important information on the subsequent compacted final product, Al_2O_3–YAG. There are few studies in which the Al_2O_3–Y_2O_3 powder mixture is pre-sintered and characterized prior to forming.

Al_2O_3 is widely used in industrial applications due to its high chemical stability and good mechanical properties, such as fracture behavior and hardness. Various additives are added to improve these properties of Al_2O_3. According to the Y_2O_3 content of these additives, in addition to Al_2O_3, YAG, and YAP phases are often obtained [7–11], where YAP represents yttrium aluminum perovskite $YAlO_3$. It has been shown that the diffraction patterns of YAG and YAP phases are identical, and that YAG is the more stable phase in the Al_2O_3–Y_2O_3 phase system [12–14].

Al_2O_3–YAG eutectic ceramics are used in high temperature applications, such as turbine blades, due to their super-

ior mechanical properties and oxidation resistance at high temperatures [15, 16]. Directionally solidified eutectic ceramics, such as Al_2O_3–YAG, do not contain grain boundaries and colonies, and therefore, have good strength properties at high temperatures [17]. Directionally solidified Al_2O_3–YAG composites are obtained by crystal growth techniques, such as micro-pulling-down [18, 19], Bridgman [20, 21] and laser-heated float zone techniques [22, 23].

Recently, polycrystalline Al_2O_3–YAG ceramics have emerged as an alternative to directionally- solidified Al_2O_3–YAG ceramics, due to lower production costs, simpler production processes, and larger size of the final product [24, 25]. Li and Gao [26] reported that the disadvantages of Al_2O_3–YAG eutectic composites obtained by the complex directionally-solidified production method, including low strength and fracture toughness at room temperature, could be turned into an advantage with polycrystalline Al_2O_3–YAG composites. In recent years, it has been shown that polycrystalline Al_2O_3–YAG eutectic ceramics produced by sintering, suitable for industrial production, have good mechanical properties [27–31]. In this study, the traditional sintering method was used in the production of Al_2O_3–YAP powder. As future work, the Al_2O_3–YAP powder used in this study will be formed and re-sintered to produce polycrystalline Al_2O_3–YAG materials.

While sintering methods in ceramic powders affect powder characteristics, thus affecting material properties, the purity and grain size of the powders also affect the sintering rate and temperature [32–34]. Cinibulk [35] studied the effects of the Y_2O_3 additive on the density and grain growth of Al_2O_3 at high temperatures, especially using direct mixing of the two powders as a sintering method. Cinibulk et al. [36] showed that YAG addition affected the pore structure of the Al_2O_3 matrix composite. Lartigue-Korinek et al. [37] studied the changes in the microstructure of the Al_2O_3 matrix composite with the addition of Y, and showed that the Y dopant affected the homogeneity of the microstructure. Egelja et al. [38] showed that compounds containing Al and Y transformed into the YAG phase at 1 100 °C. In the same study, it was determined that the amount of Al_2O_3 increased and the amount of YAG decreased at higher temperatures, indicating that the properties of materials obtained by sintering Al_2O_3–Y_2O_3 powders change with sintering temperature.

In this study, the phase composition, microstructure, and surface area analysis of the final powders obtained by sintering high-purity Al_2O_3–Y_2O_3 powder mixture at different temperatures were investigated. The effects of sintering temperature variation on material properties are discussed. The aim of this study was to obtain low porosity and uniformly microstructured YAP phase at low temperatures, to be used as a transition phase and sintering activator in the formation of a YAG structure.

Table 1. Specific features of powders.

Raw materials	Al_2O_3	Y_2O_3
Supplier	Sigma Aldrich	Alfa Aesar
Grain size (μm)	44*	<10
Purity (%)	99.99	99.999

*>149 μm %30, >74 μm %80, >44 μm %99

2 Experimental procedure

The Al_2O_3–Y_2O_3 powder mixture containing Y_2O_3 (33 wt.%) and Al_2O_3 (67 wt.%) (properties listed in Table 1) was ground in a Retsch RS 200 vibratory disc mill (Haan, Germany) at 800 rpm for 2 min. After grinding, the powders were granulated for 1 h at 1 000 °C using a Thermolyne 48 000 furnace (Barnstead International, Dubuque, IA). The powders were then dry-ground in a ball mill with Macchine Macina Smalto (MMS, Modena, Italy) for 1 h. The samples were dried at 100 °C in an oven (Memmert UF 55, Germany), and then classified with a 106 μm sieve, using a Retsch AS 200 sieve shaker (Haan, Germany). The sieved powders were weighed on a precision balance (Radwag AS 220.R2, Poland) on an electronic scale with an accuracy of ±0.1 mg, and then divided into 3 powder samples (19.5 g each).

The divided powders were loaded into crucibles (Isolab Laborgerate GmbH, Germany) and sintered in a Protherm PLF 110/8 model furnace (Alser Teknik, Turkey) at temperatures of 1 000, 1 050 and 1 100 °C, respectively. During the sintering process, the furnace was brought to the desired temperatures over 60 min, kept at sintering temperatures for 2 h, and then regressed to room temperature over 65 min. After repeating the operation for each sintering temperature, the powder samples were pulverized in a mortar, and then sieved in a vibratory sieve shaker with a 106 μm sieve for 2 min.

Phase compositions of each sample were examined using an X-ray diffractometer (XRD, PANalytical Empyrean). For analysis, the powder samples were compressed into molds without any gaps. The process was carried out using a diffractometer in the 2θ range of 10°–80° using Cu-K_α radiation. Phase quantities of Al_2O_3–Y_2O_3 mixed powders sintered at different temperatures were obtained using PANalytical HighScore Plus software, based on the Rietveld method. Scanning electron microscope (SEM, JEOL JSM7100F) analysis was performed in order to investigate the effect of temperature change on phase formation, homogeneity, grain size change, and crystallization criteria in the powder samples. Prior to SEM analysis, the powder samples were mounted onto double-sided carbon tape. In order to increase conductivity, the samples were sputter-coated with Au-Pd (80 : 20 wt.%), under 10 mA current application and 8×10^{-1} m bar atmosphere in a Quorum coating device (Polaron SC7620, Quorum Technologies, UK). Elemental analysis of the microstructurally-imaged internal structures was performed using SEM-EDS (Oxford Instruments X-Max). Surface areas, micropore size distribution, and pore volumes and sizes of the sintered powder samples were measured using a Brunauer–Emmett–Teller (BET) surface area analyzer

(Quantachrome Instruments, Quadrosorb SI, USA). Physical absorption measurements were carried out using nitrogen gas in a liquid-nitrogen environment (77 K). Prior to measurement, the samples were degassed using a degassing device (Quantachrome Instruments, Flovac Degasser, USA) at 400 °C for 2 h.

3 Results and discussion

Figure 1 shows XRD patterns of the powders of like composition sintered at 1 000, 1 050 and 1 100 °C (1000AY, 1050AY and 1100AY, respectively) from the Al_2O_3–Y_2O_3 starting material. The transformation of the Al and Y containing compounds into the YAP (JCPDS 01-074-1334) phase takes place at 1 100 °C. Although Wang and Gao [7] observed the first YAG crystallization in the solid state at a temperature near 1 000 °C, the YAG crystallization was not observed at any temperature in this study. This may be due to insufficient YAP phase present for reaction with Al_2O_3, an intermediate stage toward the emergence of the YAG phase at these temperatures. As the sintering temperature increased up to 1 100 °C, the peaks in the XRD pattern became more frequent, and a new phase was observed. YAG production from Al_2O_3–Y_2O_3 powder mixtures takes place via the reaction processes and temperatures in Eqs. (1–3), as shown in previous works [34, 39].

$$2Y_2O_3 + Al_2O_3 \rightarrow Y_4Al_2O_9\ (\mathrm{YAM}, 900\,^{\circ}\mathrm{C} - 1\,100\,^{\circ}\mathrm{C}) \quad (1)$$

$$\mathrm{YAM} + Al_2O_3 \rightarrow 4YAlO_3\ (\mathrm{YAP}, 1\,100\,^{\circ}\mathrm{C} - 1\,250\,^{\circ}\mathrm{C}) \quad (2)$$

$$3\mathrm{YAP} + Al_2O_3 \rightarrow Y_3Al_5O_{12}\ (\mathrm{YAG}, 1\,400\,^{\circ}\mathrm{C} - 1\,600\,^{\circ}\mathrm{C}) \quad (3)$$

As shown in Fig. 1, an increase in sintering temperature drives the reactions in Eqs. (1–3). The first YAM (yttrium aluminum monoclinic) structure was formed at 1 000 °C. Small peaks corresponding to the YAM (JCPDS 01-083-0933) phase emerged at 1 000 and 1 050 °C. At 1 100 °C, the amount of YAM phase increased, and the YAP phase also appeared. 1 100 °C is considered a transition temperature, where the crystallization rate increases and new phases begin to emerge. Phase quantifications of the Al_2O_3–Y_2O_3 powder

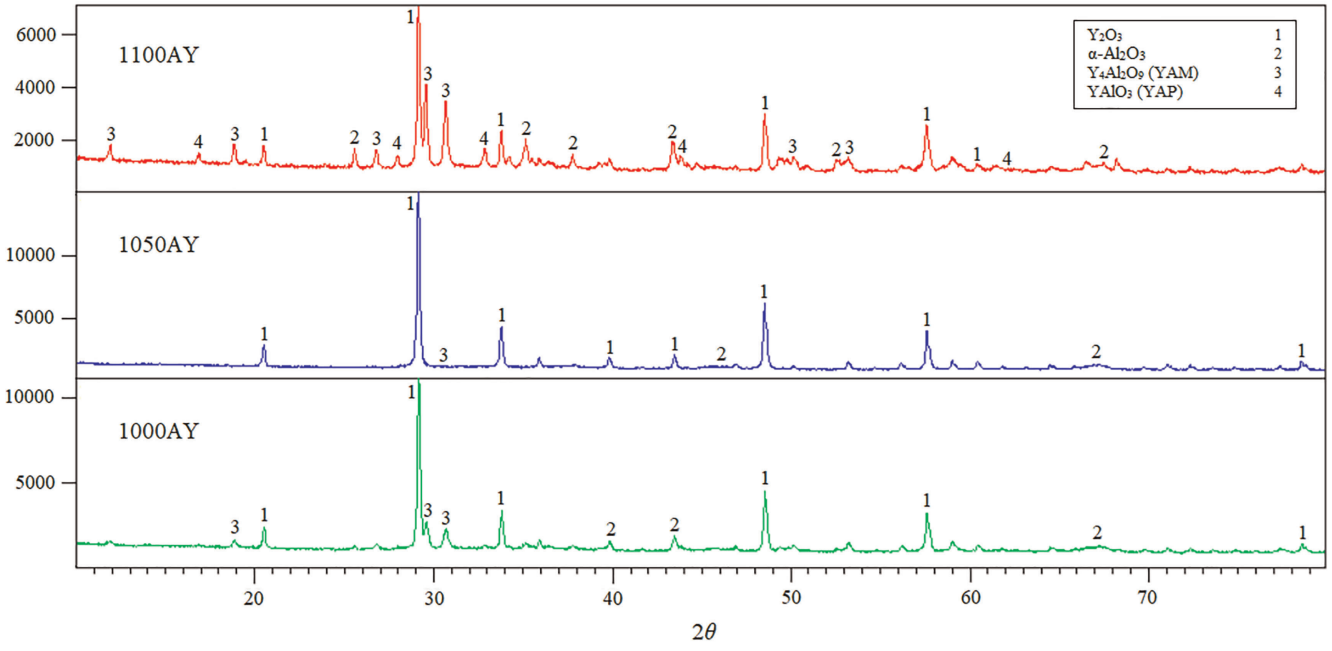

Fig. 1. XRD patterns of Al_2O_3–Y_2O_3 powders of like composition, sintered at different temperatures.

Table 2. Phase quantitative results calculated from XRD peaks of samples consisting of Al_2O_3–Y_2O_3 powders sintered at 1 000 °C, 1 050 °C, and 1 100 °C.

Temperature (°C)	Phase composition (wt.%)			
	α-Al_2O_3	Y_2O_3	$Y_4Al_2O_9$ (YAM)	$YAlO_3$ (YAP)
1 000	18.2	55.9	25.8	–
1 050	54.5	44.8	0.6	–
1 100	38.5	23	31.9	6.6

samples sintered at different temperatures are shown in Table 2. The Y_2O_3 (JCPDS 01-088-2162) phase is significantly reduced at 1 100 °C (23 wt.%), compared to samples sintered at other temperatures. At this temperature, the Y_2O_3 phase reacted further and new phases emerged. The formation of a small amount of YAM phase at 1 050 °C indicates that aluminum diffuses incompletely into Y_2O_3. Although the amount of YAM phase formed at 1 000 °C was higher than for the sample sintered at 1 050 °C, Al_2O_3 (corundum JCPDS 00-010-0173) could not crystallize significantly at 1 000 °C. There was also no significant decrease in the Y_2O_3 phase, indicating that Y_2O_3 did not significantly react at 1 050 °C. In addition, although the YAM phase was quantitatively high at 1 000 °C, the relative peak intensity was low. The YAM phase, which crystallized sufficiently at 1 100 °C, began to transform into the YAP phase. In order for the YAM phase to convert to YAP, the YAM phase must be well-crystallized, which did not occur at 1 000 °C. The low amount of YAM phase observed at 1 050 °C may be due to early stages of this crystallization. Since both the increase in YAM phase and the formation of the new YAP phase at 1 100 °C increase the amount of reactive Al_2O_3, while decreasing the amount of Al_2O_3 that converts to corundum, there was no significant decrease in corundum, compared to sintering at 1 050 °C. However, this does not mean that Al_2O_3 cannot crystallize well at 1 100 °C. At 1 100 °C, aluminum continues to diffuse into the YAM phase, but also begins to diffuse into the newly-crystallized YAP phase. Although Prnová et al. [40] determined the crystallization temperature of Al_2O_3 as 1 300 °C, this temperature was reduced under our working conditions, wherein the first Al_2O_3–YAP phase was obtained at 1 100 °C. Despite previous reports [7, 8, 38, 40] showing decreased YAG formation temperatures with according chemical processing of starting materials, Li and Gao [26] showed that temperatures of 1 300 °C and higher were required for a high-quality YAG crystal.

The SEM-EDS analyses of the powders sintered at different temperatures are shown in Fig. 2. No elements other than Al, Y, and O were observed in the powder samples sintered at all three temperatures. The results support the analysis of XRD patterns of the samples. Elemental analysis of the 1100AY powder taken from several regions in the SEM images reveal that the Al and O signals are reduced considerably, compared to the analyses of the 1000AY and 1050AY powders. This is due to the reaction of both elements to form new crystal phases (YAP and YAM). The excess Y content is also an indicator of the presence of such newly-formed phases. However, when the EDS spectrum of the powder sample sintered at 1 100 °C is examined, it is seen that the α-Al_2O_3, especially the YAP and YAM phases are formed clearly. The more distinct phase differences show that α-Al_2O_3, YAP and YAM phases are distributed more homogeneously in the powder sample sintered at 1 100 °C.

Figure 3 shows SEM images of samples 1000AY, 1050AY and 1100AY. Considering the general microstructure of sample 1100AY, it was observed that crystallization increased, and that YAP and YAM phases began to segregate from the corundum phase. In samples 1000AY and 1050AY, the YAP and YAM phases did not completely crystallize, and separate YAP, YAM, and corundum phase regions did not form. Therefore, samples 1000AY and 1050AY had non-uniform and inhomogeneous microstructures. In all samples except 1100AY, the powders are agglomerated and irregularly-shaped, and although the grain sizes cannot be clearly defined, coarser grains are noticeable in 1000AY and 1050AY compared to 1100AY. For powders sintered at 1 100 °C, spherical particles were observed. The YAP and YAM particles become embedded in the α-Al_2O_3 matrix, indicating that the Al_2O_3–YAM and Al_2O_3–YAP phases

Fig. 2. EDS spectra of Al_2O_3–Y_2O_3 powders sintered at (a) 1 000 °C, (b) 1 050 °C, and (c) 1 100 °C.

formed only at 1 100 °C, denoted as the transition temperature. No amorphous phase regions were observed in any sample. The high purity of the starting powders and the preparation of the raw materials without chemical processes are both effective in eliminating disadvantageous amorphous phases. Grain formations are observed in the SEM image of sample 1100AY. Contrary to the expected grain growth with the increase in temperature, as seen in Fig. 3, a coarse-grained structure is observed in samples 1000AY and 1050AY, and a fine-grained structure with more uniform grain sizes in sample 1100AY. This is likely due to strong intergranular bonding in 1100AY, which also causes the development of new phases in the sample sintered at 1100 °C. When the microstructure of sample 1100AY (Fig. 3c and d) is examined, a transformation at 1 100 °C into a fine particle network is observed, where the interparticle neck formation begins. In the microstructure images in Fig. 3, the particles in samples 1000AY and 1050AY have irregular boundaries and shapes, while sample 1100AY, sintered at 1 100 °C, transforms into a uniform structure with similar grain sizes. The YAP and YAM particles become embedded in the α-Al_2O_3 matrix, indicating that the Al_2O_3–YAM and Al_2O_3–YAP phases formed only at 1 100 °C, denoted as the transition temperature. Nagira et al. [41] stated that a desirable Al_2O_3–YAG phase was obtained from the Al_2O_3–YAP particle and that the quality of the Al_2O_3–YAG phase was dependent on that of the initial Al_2O_3–YAP phase, emphasizing the importance of the low amount of porous particles in the structure. Although Al_2O_3–YAP was not used as a starting material in this study, Fig. 3c and d shows the morphological structure of the Al_2O_3–YAP phase, which may react to form the Al_2O_3–YAG phase. Olmos et al. [2] observed porous structures as a result of sintering powder materials. Other reports [42, 43] showed that porous structures emerged due to exceeding the solubility limit of yttrium during formation of the YAP and YAG phases. The amount of doped Y_2O_3 in this study does not exceed the solubility limit of yttrium [9, 44, 45]. When the images in Fig. 3 are examined, no sig-

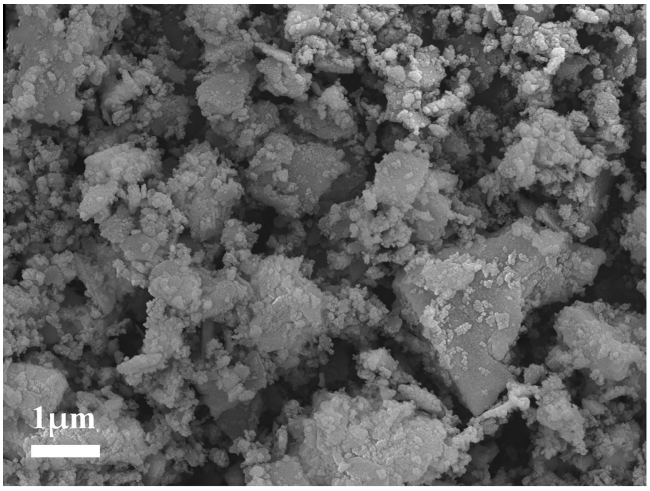

(a)

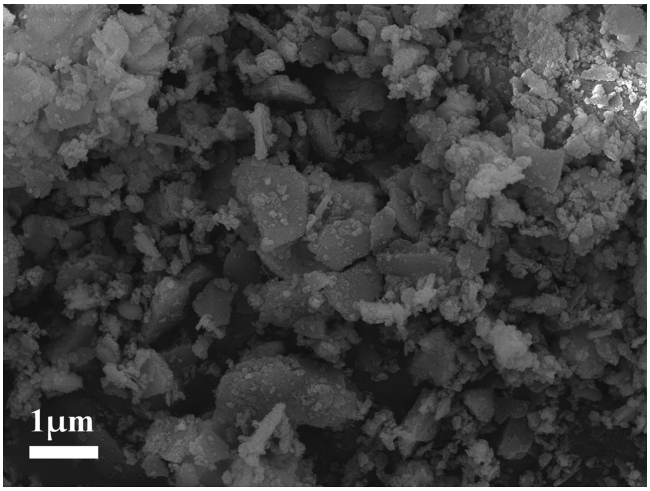

(b)

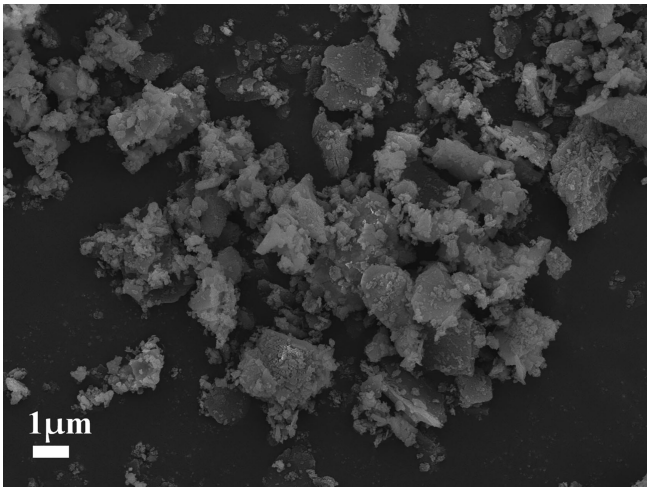

(c)

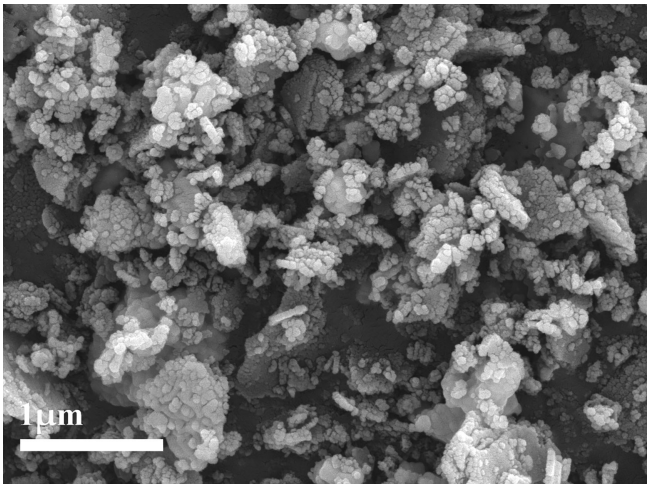

(d)

Fig. 3. SEM microstructural analysis of Al_2O_3–Y_2O_3 powders sintered at (a) 1 000 °C, (b) 1 050 °C, and (c, d) 1 100 °C.

nificant pore formation in any sample after sintering is observed. In samples 1000AY and 1050AY, there is no pore formation, since YAP formation does not occur. However, the absence of a significant pore problem in the 1100AY sample, which we consider as the transition temperature, shows that there is no excess solubility that will cause blocking of the grain boundaries and excessive pore formation. Towata et al. [43] showed that the formation of Al_2O_3–YAP fiber–matrix composite structure prevents grain growth that causes the emergence of excessive porous structures, which may explain the results in this report.

BET specific surface areas of the powder samples sintered at all three temperatures are shown in Table 3. Within the range tested, pore size is not significantly affected

Table 3. Microstructural surface analysis results of Al_2O_3–Y_2O_3 powders sintered at different temperatures.

Temperature (°C)	Surface area ($m^2\ g^{-1}$)	Average pore size (nm)	Pore volume ($cm^3\ g^{-1}$)
1 000	56.84	5.70	0.087
1 050	91.29	4.74	0.117
1 100	33.29	5.45	0.050

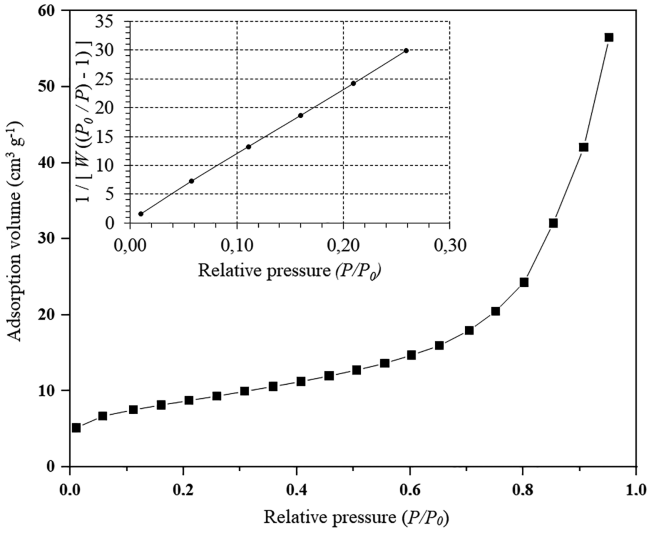

(a)

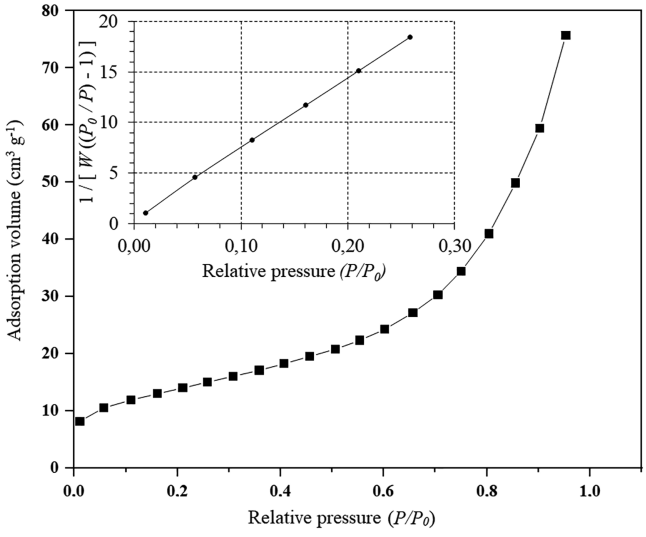

(b)

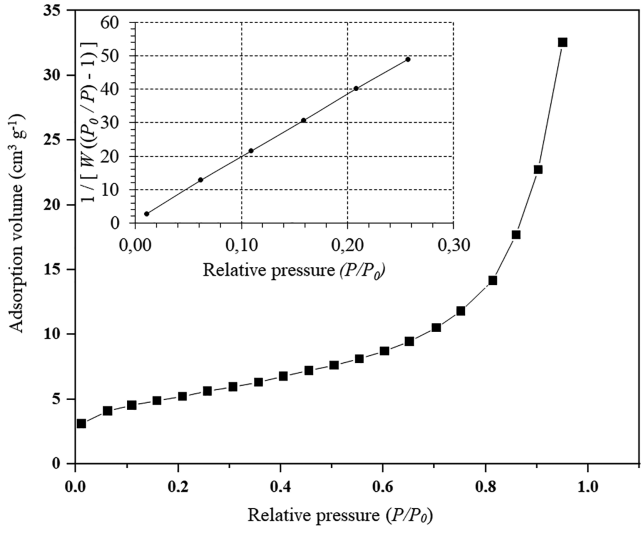

(c)

Fig. 4. Nitrogen absorption isotherms of Al_2O_3–Y_2O_3 powders sintered at (a) 1 000 °C, (b) 1 050 °C, and (c) 1 100 °C.

by temperature. Sample 1100AY has the lowest surface area and pore volume; therefore, powders sintered at 1 100 °C have lower porosity, which is desirable for eutectic ceramic composites. Although sample 1050AY is sintered at higher temperature, there is an increase in the surface area compared to sample 1000AY, and thus, the temperature at which porosity is eliminated is not reached. The BET measurements of sample 1100AY are consistent with the results of Towata et al. [43], which showed that sufficiently-crystallized composite structures inhibit grain growth and porosity. However, the low pore volume of the 1100AY sample prevents the formation of clustered pores and provides a more uniform structure [46]. This result is consistent with SEM analysis of sample 1100AY, as seen in Fig. 3. Figure 4 shows the adsorption isotherms of the powder samples sintered at all three temperatures. The adsorption isotherms are type II isotherms, according to the IUPAC classification [47]. A combination of type II and type IV isotherms exists at low relative pressures($P/P_0 = 0 - 0.70$). As both pore volume and specific surface area of sample 1100AY were lower than in the other two samples (Table 3), the adsorption rate in sample 1100AY was lower than for samples 1000AY and 1050AY. Adsorption is also low at low pressures in all three samples. Adsorption values within the $P/P_0 = 0.05 - 0.30$ relative pressure range indicate the presence of micropores [48]. As the pressure increases, the adsorption also increases slowly. When the relative pressure reaches approximately 0.90, a sudden increase in the rate of adsorption occurs. Thus, all three samples have microporous and mesoporous structures [49]. The average pore sizes of all three samples (Table 3) show that the sintered samples are dominated by mesopores. The adsorption rates at low pressures in samples 1000AY and 1050AY are slightly higher than in sample 1100AY. Thus, the micropore volume in sample 1100AY decreased compared to the other two samples. In addition, the lower adsorption of sample 1100AY in the micropore regions, where a linear plot is obtained in the multipoint BET graphs (Fig. 4), confirms the presence of fewer micropores. The reason for the increase in pore size in the high-temperature sample 1100AY, which contributes to mesopore formation with the decrease in the specific surface area, may be the removal of materials from the convex grain to more concave necks [50]. Microporous powder structures can cause crack propagation in rigid structures during the subsequent forming processes [51]. Due to the low open porosity in compact structures formed and sintered from less microporous powder, the fragility of materials at high temperatures may decrease. However, the mesoporous structure in sample 1100AY is another factor which explains its homogeneous pore distribution [52]. It is known that the pore struc-

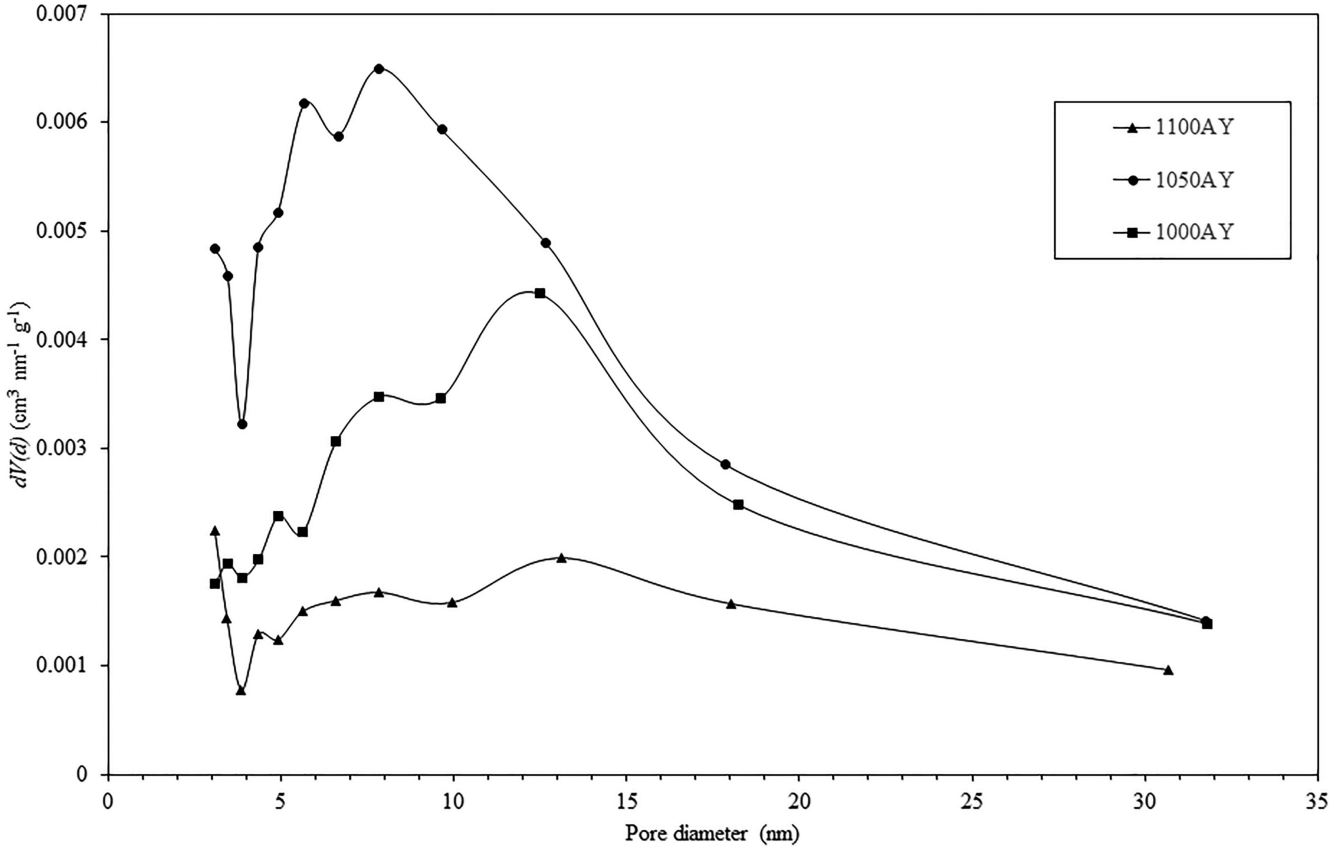

Fig. 5. BJH pore size distributions of Al_2O_3–Y_2O_3 powders sintered at different temperatures.

ture in powder materials affects the mechanical properties of the final product [53, 54]. According to these studies, it is expected that the rigid structure obtained from the 1100AY powder sample, which has lower microporosity compared to samples 1000AY and 1050AY, will be more resistant to microcracks. As seen in Fig. 5, all three samples give a Barrett–Joyner–Halenda (BJH) pore size distribution compatible with BET average pore sizes and pore volumes (Table 3). Micropores are not seen in BJH measurements, as the relative pressure range of 0 – 0.35 is not probed. As seen in Fig. 5, there is a sharp peak between 5 – 10 nm for sample 1050AY, while other samples have a smaller but distinct peak in the same range. A sharp peak is seen in the 10 – 15 nm range in sample 1000AY and in the 10 – 18 nm in sample 1100AY. Sample 1100AY contains large mesopores in a wide range of pore sizes. The wide range of pore sizes seen in sample 1100AY is due to the difference in the amount of small and large size pores in its microstructure, compared to samples 1000AY and 1050AY. Pore size distribution graphs show that sample 1100AY has fewer small mesopores or micropores and more large-sized mesopores, confirming the isotherm curves. In addition, considering each pore size for the 1100AY sample, there is a unimodal distribution wherein the difference between decreasing and increasing peaks is less. A bimodal distribution is observed for 1000AY and 1050AY samples. The minor difference between peak intensities for the 1100AY sample indicates that the distribution in all pore sizes is homogeneous.

4 Conclusions

The optimum temperature required for the crystallization of YAP from YAM and Al_2O_3 processing is 1 100 °C, which occurs as a result of the chemical reactions between Al_2O_3 and Y_2O_3 powders during sintering. From mineralogical and microstructural analysis of the powder sintered at 1 100 °C, it was determined that Al_2O_3–YAP powder was produced. The powder sintered at 1 100 °C is composed of a uniform structure, and contains particles with low, homogeneously-distributed porosity, and forms a desirable composite material. Al_2O_3–YAP powder will be used as a raw material in the future to obtain compact polycrystalline Al_2O_3–YAG which is dual-phase at lower temperatures and more crystallized.

Funding: This study was supported by Çanakkale Onsekiz Mart University Science and Technology Application and Research Center (COBILTUM).

References

[1] Y. Waku, N. Nakagawa, T. Wakamoto, H. Ohtsubo, K. Shimizu, Y. Kohtoku: J. Mater. Sci. 33 (1998) 1217. DOI:10.1023/A:1004377626345
[2] L. Olmos, C.L. Martin, D. Bouvard: Powder Technol. 190 (2009) 134. DOI:10.1016/j.powtec.2008.04.057
[3] D. Bouvard: Powder Technol. 111 (2000) 231. DOI:10.1016/s0032-5910(99)00293-4
[4] Q. Zhang, F. Saito: Powder Technol. 129 (2003) 86. DOI:10.1016/S0032-5910(02)00136-5
[5] B. Lin, D. Yi, H. Liu, J. Xu, B. Wang: J. Alloys Compd. 814 (2020) 152325. DOI:10.1016/j.jallcom.2019.152325
[6] Y. Yu, W. Zhang, W. Dong, J. Yang, Y. Feng: Mat. Sci. Eng. A-Struct. 638 (2015) 38. DOI:10.1016/j.msea.2015.04.050
[7] H. Wang, L. Gao: Ceram. Int. 27 (2001) 721. DOI:10.1016/S0272-8842(01)00009-8
[8] P. Palmero, A. Simone, C. Esnouf, G. Fantozzi, L. Montanaro: J. Eur. Ceram. Soc. 26 (2006) 941. DOI:10.1016/j.jeurceramsoc.2004.12.020
[9] H. Yasuda, I. Ohnaka, Y. Mizutani, A. Sugiyama, T. Morikawa, S. Takeshima, T. Sakimura, Y. Waku: Sci. Technol. Adv. Mat. 5 (2004) 207. DOI:10.1016/j.stam.2003.10.022
[10] H. Yasuda, Y. Mizutani, I. Ohnaka, A. Sugiyama, Y. Waku: Mater. Trans. 42 (2001) 2124. DOI:10.2320/matertrans.42.2124
[11] S. Abalı, C.U. Karaçam: Proceedings 2 (2018) 1407. DOI:10.3390/proceedings2231407
[12] J.S. Abell, I.R. Harris, B. Cockayne, B. Lent: J. Mater. Sci. 9 (1974) 527. DOI:10.1007/BF00551870
[13] B. Cockayne: J. Less-Common Met. 114 (1985) 199. DOI:10.1016/0022-5088(85)90402-3
[14] M. Medraj, R. Hammond, M.A. Parvez, R.A.L. Drew, W.T. Thompson: J. Eur. Ceram. Soc. 26 (2006) 3515. DOI:10.1016/j.jeurceramsoc.2005.12.008
[15] D. Liu, Y. Gao, J. Liu, F. Liu, K. Li, H. Su, Y. Wang, L. An: Scripta Mater. 114 (2016) 108. DOI:10.1016/j.scriptamat.2015.12.002
[16] J. Llorca, V. Orera: Prog. Mater. Sci. 51 (2006) 711. DOI:10.1016/j.pmatsci.2005.10.002
[17] N. Nakagawa, H. Ohtsubo, A. Mitani, K. Shimizu, Y. Waku: J. Eur. Ceram. Soc. 25 (2005) 1251. DOI:10.1016/j.jeurceramsoc.2005.01.030
[18] A. Yoshikawa, B.M. Epelbaum, T. Fukuda, K. Suzuki, Y. Waku: Jpn. J. Appl. Phys. 38 (1999) L55. DOI:10.1143/JJAP.38.L55
[19] Y. Mizutani, H. Yasuda, I. Ohnaka, N. Maeda, Y. Waku: J. Cryst. Growth 244 (2002) 384. DOI:10.1016/S0022-0248(02)01655-X
[20] F. Schmid, D. Viechnicki: J. Mater. Sci. 5 (1970) 470. DOI:10.1007/BF00556032
[21] Y. Waku, N. Nakagawa, T. Wakamoto, H. Ohtsubo, K. Shimizu, Y. Kohtoku: J. Mate.r Sci. 33 (1998) 4943. DOI:10.1023/A:1004486303958
[22] C.S. Frazer, E.C. Dickey, A. Sayir: J. Cryst. Growth 233 (2001) 187. DOI:10.1016/S0022-0248(01)01590-1
[23] M.C. Mesa, P.B. Oliete, V.M. Orera, J.Y. Pastor, A. Martín, J. Llorca: J. Eur. Ceram. Soc. 31 (2011) 1241. DOI:10.1016/j.jeurceramsoc.2010.05.004
[24] E.S. Lima, L.H.L. Louro, J.B. de Campos, R.R. de Avillez, C.A. Costa, in: Proceedings of the EUROPM2007, European Powder Metallurgy Association, Shrewsbury (2007) 89.
[25] C. Oelgardt, J. Anderson, J.G. Heinrich, G.L. Messing: J. Eur. Ceram. Soc. 30 (2010) 649. DOI:10.1016/j.jeurceramsoc.2009.09.011
[26] W.Q. Li, L. Gao: Nanostruct. Mater. 11 (1999) 1073. DOI:10.1016/S0965-9773(99)00396-7
[27] R. Lach, K. Haberko, B. Trybalska: Process. Appl. Ceram. 4 (2010) 1. DOI:10.2298/PAC1001001L
[28] H. Wang, L. Gao, Z. Shen, M. Nygren: J. Eur. Ceram. Soc. 21 (2001) 779. DOI:10.1016/S0955-2219(00)00262-4
[29] R. Lach, K. Haberko, M.M. Bućko, M. Szumera, G. Grabowski: J. Eur. Ceram. Soc. 31 (2011) 1889. DOI:10.1016/j.jeurceramsoc.2011.04.003
[30] P. Palmero, G. Fantozzi, F. Lomello, G. Bonnefont, L. Montanaro: Ceram. Int. 38 (2012) 433. DOI:10.1016/j.ceramint.2011.07.024
[31] E. de Souza Lima, L.H.L. Louro, R. de Freitas Cabral, J.B. de Campos, R.R. de Avillez, C.A. Da Costa: J. Mater. Res. Technol. 2 (2013) 18. DOI:10.1016/j.jmrt.2013.03.005
[32] F. Sommer, F. Kern, H.F. El-Maghraby, M.A. El-Ezz, M. Awaad, R. Gadow, S.M. Naga: Ceram. Int. 38 (2012) 4819. DOI:10.1016/j.ceramint.2012.02.070
[33] J. Markmann, A. Tschöpe, R. Birringer: Acta Mater. 50 (2002) 1433. DOI:10.1016/S1359-6454(01)00448-7

[34] J.-G. Li, J.-H. Lee, T. Mori, Y. Yajima, S. Takenouchi, T. Ikegami: J. Ceram. Soc. Jpn. 108 (2000) 439. DOI:10.2109/jcersj.108.1257_439
[35] M.K. Cinibulk: J. Am. Ceram. Soc. 87 (2004) 692. DOI:10.1111/j.1551-2916.2004.00692.x
[36] M.K. Cinibulk, K.A. Keller, T.-I. Mah: J. Am. Ceram. Soc. 87 (2004) 881. DOI:10.1111/j.1551-2916.2004.00881.x
[37] S. Lartigue-Korinek, C. Carry, L. Priester: J. Eur. Ceram. Soc. 22 (2002) 1525. DOI:10.1016/S0955-2219(01)00471-X
[38] A. Egelja, J. Majstorovic, N. Vukovic, M. Stankovic, D. Bucevac: Sci. Sinter. 48 (2016) 303. DOI:10.2298/SOS1603303E
[39] L. Wen, X. Sun, Z. Xiu, S. Chen, C.-T. Tsai: J. Eur. Ceram. Soc. 24 (2004) 2681. DOI:10.1016/j.jeurceramsoc.2003.09.001
[40] A. Prnová, J. Valúchová, M. Parchovianský, W. Wisniewski, P. Švančárek, R. Klement, Ľ. Hric, E. Bruneel, D. Galusek: J. Eur. Ceram. Soc. 40 (2020) 852. DOI:10.1016/j.jeurceramsoc.2019.10.017
[41] T. Nagira, H. Yasuda, T. Sakimura, A. Kawaguchi: Mater. Trans. 48 (2007) 2312. DOI:10.2320/matertrans.MB200705
[42] S.A. Hassanzadeh-Tabrizi, E. Taheri-Nassaj: J. Alloy. Compd. 506 (2010) 640. DOI:10.1016/j.jallcom.2010.07.030
[43] A. Towata, H.J. Hwang, M. Yasuoka, M. Sando, K. Niihara: J. Am. Ceram. Soc. 81 (1998) 2469. DOI:10.1111/j.1151-2916.1998.tb02645.x
[44] H. Yasuda, I. Ohnaka, Y. Mizutani, Y. Waku: Sci. Technol. Adv. Mat. 2 (2001) 67. DOI:10.1016/S1468-6996(01)00027-4
[45] F.J. Paneto, J.L. Pereira, J.O. Lima, E.J. Jesus, L.A. Silva, E. Sousa Lima, R.F. Cabral, C. Santos: Int. J. Refract. Met. H. 48 (2015) 365. DOI:10.1016/j.ijrmhm.2014.09.010
[46] J. Yu, J.C. Yu, M.K.-P. Leung, W. Ho, B. Cheng, X. Zhao, J. Zhao: J. Catal. 217 (2003) 69. DOI:10.1016/S0021-9517(03)00034-4
[47] K.S.W. Sing: Pure Appl. Chem. 57 (1985) 603. DOI:10.1351/pac198557040603
[48] K.C. Kim, T.-U. Yoon, Y.-S. Bae: Micropor. Mesopor. Mat. 224 (2016) 294. DOI:10.1016/j.micromeso.2016.01.003
[49] Y. Liu, W. Wang, A. Wang: Powder Technol. 225 (2012) 124. DOI:10.1016/j.powtec.2012.03.049
[50] J. Choi, J. Kim, K.S. Yoo, T.G. Lee: Powder Technol. 181 (2008) 83. DOI:10.1016/j.powtec.2007.06.022
[51] Z. Chen, W. Yan, Y. Dai, S. Schafföner, B. Han, N, Li: Ceram. Int. 45 (2019) 8533. DOI:10.1016/j.ceramint.2019.01.168
[52] H.-J. Liu, J. Wang, C.-X. Wang, Y.-Y. Xia: Adv. Energy Mater. 1 (2011) 1101. DOI:10.1002/aenm.201100255
[53] A. Kocjan, T. Konegger, A. Dakskobler: J. Mater. Sci. 52 (2017) 11168. DOI:10.1007/s10853-017-0894-z
[54] W. Klinthong, C.-H Huang, C.-S Tan: Ind. Eng. Chem. Res. 55 (2016) 6481. DOI:10.1021/acs.iecr.6b00644

(Received September 30, 2020; accepted February 25, 2021; online since May 8, 2021)

Correspondence address

Dr. Serkan Abali
Department of Materials Science and Engineering
Çanakkale Onsekiz Mart University
Çanakkale 17100
Turkey
Tel.: +90 286 218 00 18-21045
E-mail: sabali@comu.edu.tr

Bibliography
DOI 10.1515/ijmr-2020-8106
Int. J. Mater. Res. 112 (2021) 6; page 430–438

ISSN 1862-5282 · e-ISSN 2195-8556